Structural transformation in supercooled water controls the crystallization rate of ice

Emily B. Moore[1] & Valeria Molinero[1]

One of water's unsolved puzzles is the question of what determines the lowest temperature to which it can be cooled before freezing to ice. The supercooled liquid has been probed experimentally to near the homogeneous nucleation temperature, $T_H \approx 232\,K$, yet the mechanism of ice crystallization—including the size and structure of critical nuclei—has not yet been resolved. The heat capacity and compressibility of liquid water anomalously increase on moving into the supercooled region, according to power laws that would diverge (that is, approach infinity) at $\sim 225\,K$ (refs 1, 2), so there may be a link between water's thermodynamic anomalies and the crystallization rate of ice. But probing this link is challenging because fast crystallization prevents experimental studies of the liquid below T_H. And although atomistic studies have captured water crystallization[3], high computational costs have so far prevented an assessment of the rates and mechanism involved. Here we report coarse-grained molecular simulations with the mW water model[4] in the supercooled regime around T_H which reveal that a sharp increase in the fraction of four-coordinated molecules in supercooled liquid water explains its anomalous thermodynamics and also controls the rate and mechanisms of ice formation. The results of the simulations and classical nucleation theory using experimental data suggest that the crystallization rate of water reaches a maximum around 225 K, below which ice nuclei form faster than liquid water can equilibrate. This implies a lower limit of metastability of liquid water just below T_H and well above its glass transition temperature, 136 K. By establishing a relationship between the structural transformation in liquid water and its anomalous thermodynamics and crystallization rate, our findings also provide mechanistic insight into the observed[5] dependence of homogeneous ice nucleation rates on the thermodynamics of water.

We performed large-scale molecular dynamics simulations with the mW water model, which represents a water molecule as a single particle with short-range anisotropic interactions that mimic hydrogen bonds[4], to determine the temperature dependence of key thermodynamic properties of liquid water. Figure 1a presents the enthalpy, the heat capacity and the excess free energy with respect to ice, as liquid water is cooled at the lowest rate that still produces low-density amorphous ice (LDA) in simulations with the mW water model. We note that in our simulations most molecules in LDA are four-coordinated, as in ice albeit without long-range order[6,7], and that the structural transformation from liquid water to amorphous ice is sharp but continuous. This sharp yet continuous nature of the structural transition agrees with the conclusions from experiments on water confined in narrow silica nanopores that prevent ice crystallization[8] and from a thermodynamic analysis[9] of bulk water outside the so-called 'no-man's land' that stretches between the glass transition temperature (T_g) and T_H.

The enthalpy of liquid water (Fig. 1a, top panel) decreases steeply around the liquid transformation temperature $T_L = 202 \pm 2\,K$ (defined by the maximum change in density) and approaches the value for ice (Supplementary Fig. 1). The heat capacity C_p (Fig. 1a, middle panel) reaches a maximum at T_L, which is also the locus of maximum change

in tetrahedrality and fraction of four-coordinated molecules[7]. We note that T_L in the simulations is $\sim 15\,K$ above the singular temperature of the power law, T_s, predicted by a fit of C_p obtained with the mW water[4], and $\sim 25\,K$ below the $T_s \approx 225\,K$, estimated from the experimental C_p of water[1,2]. Large patches of four-coordinated molecules—the signature of LDA, and in an earlier simulation[3] identified as the precursor of the ice nucleus—develop in supercooled water and grow on cooling following a power law that would peak at T_L (ref. 7); recent small angle X-ray scattering experiments on supercooled water down to 250 K (ref. 10) concur with our simulation results.

The development of crystallinity in water on cooling is illustrated in Fig. 1b. We note that calorimetry and X-ray diffraction report 5% ice in LDA[11], which is the same fraction we find in our simulations (Supplementary Fig. 2). We also find that ice in LDA appears as small crystallites surrounded by threads of water with a local structure intermediate between ice and the four-coordinated liquid, and without long-range order. This 'intermediate-ice' structure accounts for $\sim 20\%$ of all the water present in LDA (Supplementary Fig. 2) and may be a realization of the 'gossamer percolative network' of nanocrystallites predicted to form at temperatures for which the length scale for motions relevant to the structural relaxation of the liquid is larger than the critical nucleus size for crystallization[12]. The large number of threads of intermediate-ice that appear on approaching and crossing T_L illustrates a blurring of the boundary between clearly liquid structures and clearly crystalline structures in deeply supercooled water. Below we show that this blurring heralds the effective limit of metastability of liquid water.

Experimentally observed crystallization rates increase when cooling liquid water towards T_H but increase on heating the glass around T_g, implying the existence of a temperature T_x of maximum crystallization rate in water's 'no-man's land'. The top panel of Fig. 1a indicates that on decreasing the rate of cooling, crystallization—evidenced by a sharp decrease in enthalpy—first occurs at T_L and should thus be fastest at that temperature. Figure 2a presents the time–temperature–transformation (TTT) diagram of mW water; the circles indicate the ice crystallization times, τ_x, computed from more than 1,000 independent simulations. The data show that τ_x is minimum at $T_x \approx 200\,K$, almost identical to $T_L = 202 \pm 2\,K$. For comparison, Fig. 2b shows the TTT curve obtained when using nucleation theory and experimental data for water (Supplementary discussion A): the crystallization time τ_x is predicted to be minimum and the crystallization rate maximum at $T_x \approx 225\,K$, close to T_s and just a few degrees below T_H.

To disentangle the contributions of structural transformation and degree of supercooling in determining T_x, we investigated the freezing of water that is confined in a 3-nm-diameter cylindrical nanopore and therefore exhibits a decrease in the melting temperature of ice from 273 to 220 K for both the mW model[13] and experiment[14]. The simulations indicate that $T_L \approx T_x \approx 200\,K$ in the pore (Supplementary Fig. 3). We conclude that the freezing temperature of water is controlled by the structural transformation of the liquid and not merely the degree of supercooling. This explains the experimentally observed closing of the

[1]Department of Chemistry, University of Utah, Salt Lake City, Utah 84112-0580, USA.
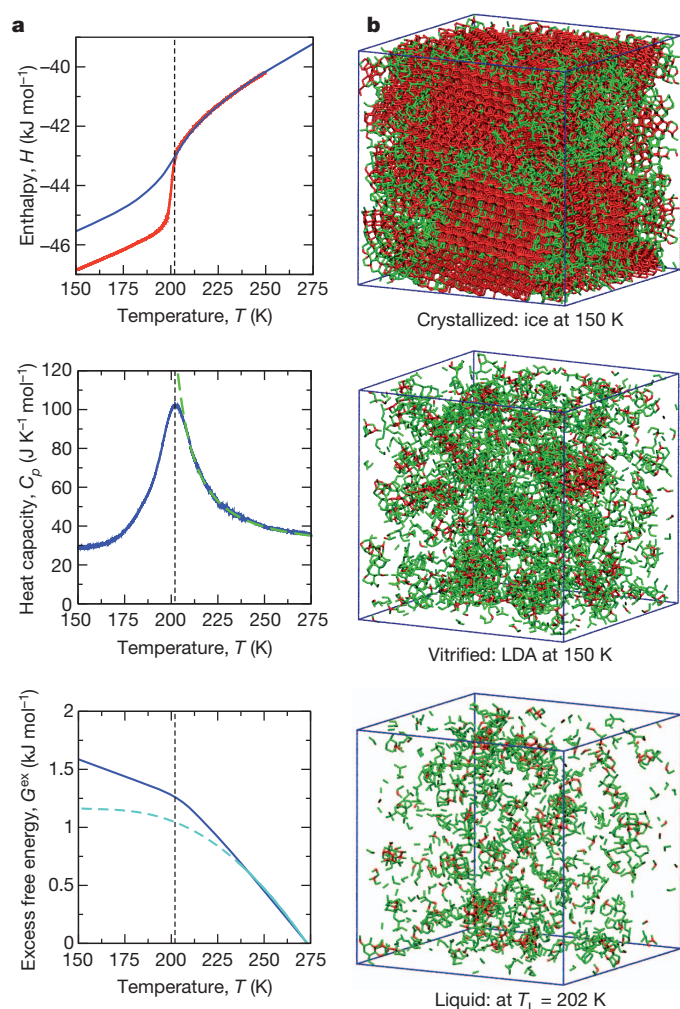
Figure 1 | Evolution of the thermodynamics and structure of water on cooling. a, Enthalpy H (top panel), heat capacity C_p (middle) and excess free energy G^{ex} (bottom) of liquid mW water on hyperquenching to LDA glass at $10\,K\,ns^{-1}$ (blue solid lines). Vertical dashed line indicates the liquid transformation temperature T_L, which sets a lower limit of metastability (LLM) of liquid water. Thus H, C_p and G^{ex} for $T < T_L$ are not equilibrium quantities and depend on the cooling rate. Cooling mW water at $1\,K\,ns^{-1}$ (red line, top) results in crystallization at T_L where the crystallization rate is maximum. On cooling towards T_L, C_p follows a power law (green dashed line, middle)[4] with exponent 1.5 as in experiments[2] and T_s about 35 K lower. G^{ex} in the simulations (blue line, bottom) is in excellent agreement with G^{ex} in experiments (solid cyan line)[9]; the dashed cyan line shows the experimental G^{ex} extrapolated below T_H (ref. 5). **b,** Ice (red) and intermediate-ice (green) in: ice formed by cooling water at $1\,K\,ns^{-1}$ (top), LDA formed by quenching water at $10\,K\,ns^{-1}$ (middle) and in liquid water at T_L (bottom). Lines connect water molecules within 3.5 Å.

gap between freezing and melting of confined water on decreasing the radius of the confining nanopore[14].

We also determined the number of water molecules N^* in the critical ice nuclei (including their sheath of intermediate-ice) through the mean first passage time (MFPT) method[15]. Our values of N^* ($\sim$120 at $T_L + 6\,K$ and $\sim$90 at $T_L + 3\,K$) are in good agreement with N^* (70–210) deduced from freezing of water in micelles around T_H (ref. 16). The critical nucleus size is determined by liquid–ice thermodynamics, well reproduced by the mW model (Supplementary discussions B and C). Critical nuclei around $T_L + 3\,K$ have a broad distribution of shapes (Fig. 2c), indicating a lowering of the ice–liquid surface tension as the structural gap between ice and liquid narrows on approaching T_L. The fraction of four-coordinated water molecules in the liquid wetting the nuclei at $T_L + 3\,K$ is 50% larger than the average for the whole liquid (Supplementary Fig. 4); this corroborates the conjecture put forward in
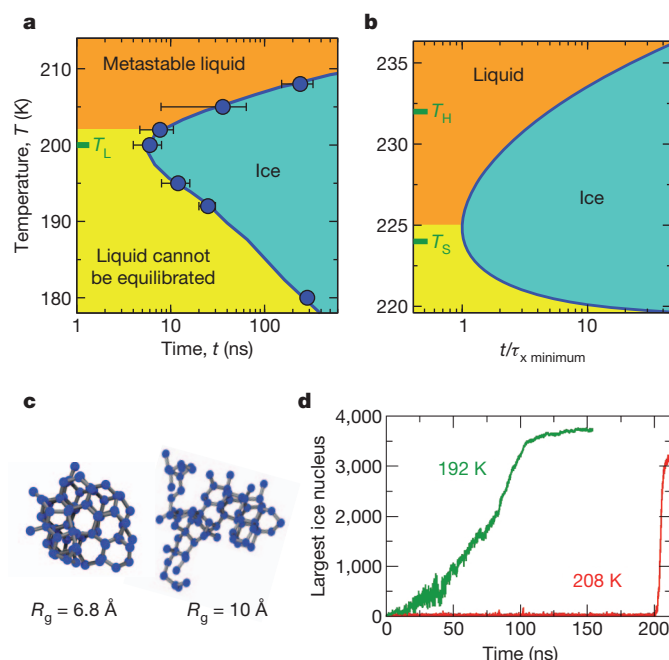
Figure 2 | Kinetics of ice crystallization and critical ice nuclei. a, Time–temperature transformation (TTT) diagram of mW water. Blue circles indicate average times τ_x to crystallize 70% of water. The error bars indicate the range of crystallization times measured in the simulations and show a large dispersion of crystallization times above T_L due to the stochastic nature of the nucleation process. Water crystallizes within the 'nose' (the blue-shaded area). The crystallization time is the shortest around 200 K, close to $T_L = 202 \pm 2\,K$. Nucleation and growth times become comparable at T_L (Supplementary Fig. 5). Above T_L, crystallization is limited by the rare formation of critical ice nuclei and supercooled water can be studied in the metastable liquid state (orange shaded area). Below T_L, crystallization occurs before relaxation of liquid water and the liquid exists only for times too short for its equilibration (yellow shaded area). The maximum crystallization rate predicted by the mW model is $J = (\tau_x V)^{-1} \approx 10^{27}\,cm^{-3}\,s^{-1}$, several orders of magnitude faster than measured for water down to T_H, because crystallization rates are proportional to water mobility (Supplementary Information section A), which is overestimated by the mW model[4,27]. **b,** TTT curve predicted using classical nucleation theory and experimental data for water. The x axis represents the time normalized by the minimum value of the crystallization time, $\tau_{x,minimum}$. The nose resulting from crossover between nucleation and growth occurs at 225 K, between the experimental T_H and T_s. The colour code of the shaded areas is the same as in **a**. **c,** Critical ice nuclei at the lowest temperature for which liquid water can be equilibrated, $T_L + 3 = 205\,K$ in the simulations, contain $\sim$90 water molecules and a wide range of compactness. The spread in the radius of gyration (R_g) of the nuclei (Supplementary Figs 6 and 7) suggests that the liquid–ice surface tension is very low on approaching T_L. **d,** Number of molecules in the largest ice nucleus for representative simulations at 208 K (red line; at this temperature, crystallization is dominated by stochastic nucleation) and at 192 K (green line; where nucleation is fast and crystallization proceeds at the pace of growth).

an earlier study[3] and suggests that four-coordinated water patches that form in the supercooled liquid stabilize the crystal nuclei.

The minimum in crystallization times around T_L signals a crossover in the mechanism of ice crystallization, from nucleation-dominated above T_L to growth-dominated below T_L (Fig. 2d). The lack of a well-defined nucleation plateau in the MFPT plot at T_L (Supplementary Fig. 5) is evidence of concurrent nucleation and growth, and implies that the barrier for nucleation is comparable to the thermal energy, RT (where R is the gas constant; Supplementary discussion D)[15]. The growth time of the crystallites is comparable to or shorter than the relaxation time of the liquid because the growth rate is proportional to the diffusivity of supercooled liquid water[17], which decouples from the structural relaxation[18] (Supplementary discussions A and D). Thus liquid water cannot be equilibrated in the simulations at $T < T_L + 3\,K$: ice nucleates before the liquid has time to equilibrate. We conclude that

the structural transformation in supercooled water around T_L sets the effective lower limit of metastability (LLM) of supercooled water.

In fact, a kinetic limit of stability for the liquid state was anticipated by Kauzmann[19], as the resolution of his entropy paradox: "the barrier to crystal nucleus formation, which tends to be very large just below the melting point, may at low temperatures be reduced to approximately the same height as the free energy barriers which impede molecular reorientations in the liquid (...). Under these circumstances crystal nuclei will form and grow at about the same rate as the liquid changes its structure following a change in temperature or pressure." An extension of this argument considered the decoupling of diffusion and viscosity in supercooled liquids and concluded that an LLM must be reached at $T_{LLM} > T_o$, where the latter indicates the temperature at which the excess entropy of the liquid would become lower than the entropy of the crystal[17]. The experimental power-law increase in C_p of liquid water on cooling supports the existence of an LLM of water between $T_{LLM} > T_o \approx T_s \approx 225\,K$ and $T_H \approx 232\,K$ (Supplementary discussions A and D); our analysis concurs with the prediction of a kinetic spinodal in water at $\sim230\,K$ based on the fluctuation theory of relaxation of metastable states[20].

The above arguments for real water, using classical nucleation theory and experimental data, predict a lower limit of metastability close to the 'nose' of the TTT curve, between T_s and T_H—as predicted by our simulations. We therefore conclude that between T_{LLM} ($\approx T_L > T_s$) and T_g, liquid water is not metastable and can only be studied over times shorter than needed for its equilibration. The low nucleation barriers and considerable water diffusivity around T_{LLM} make partial crystallization unavoidable, even at the fastest attainable cooling rates. Therefore the glass transition of LDA at $T_g \approx 136\,K$ does not produce metastable liquid water, but rather a less viscous liquid unable to relax before crystallizing. The lack of ergodicity in liquid water below $\sim225\,K$ may explain the feeble heat capacity signature at T_g that puzzled scientists for decades[21].

Various theoretical scenarios, involving a retracing spinodal of superheated water, a first-order and a continuous liquid–liquid transition, have been proposed to explain the thermodynamic anomalies of water and predict its fate in 'no-man's land'[21–25]. These scenarios assume that metastable liquid water exists below T_H. The results of the present work suggest that the structural transformation that causes the anomalies of water is also responsible for the demise of the liquid state. Water has been proposed to first convert to low-density liquid (LDL) and then crystallize[26], but our results (reported here and in ref. 27) suggest that crystallization occurs faster than LDL's equilibration. It has been argued that LDL can be equilibrated in simulations using the ST2 model[23,28]; recently reported free energy maps of ST2 and mW models, however, do not display a basin for LDL[29]. We also note that our calculations indicate that water crystallization in 'no-man's land' is limited only by the growth rate of the crystallites, which decreases on cooling. So extrapolation of crystallization rates from the nucleation-dominated region above T_H to temperatures below 225 K—that is, to temperatures relevant for cloud formation and crucial for the formulation of climate models—would severely overestimate the rates of ice formation.

METHODS SUMMARY

Simulations were performed with LAMMPS[30] using the mW water model[4], which reproduces the structure, anomalies and phase behaviour of water at less than 1% of the computational cost of atomistic models (Supplementary discussion B). Thermodynamic properties of the liquid were computed as indicated in Online Methods for simulation cells containing 32,768 molecules at pressure $p = 1$ atm and a linear decrease in temperature at $10\,K\,ns^{-1}$. Ice was identified with the CHILL algorithm[13]. Crystallization times indicate average times to crystallize 70% of ~150 independent constant pressure and temperature simulations with 4,096 molecules at each temperature. Nucleation times and the average critical size and radius of gyration of the nuclei were determined from MFPT analysis[15] of the crystallization trajectories. Identification of individual critical nuclei was performed through evaluation of their individual crystallization probability over 200 independent simulations for each nucleus, starting with the same configuration and randomized momenta.

1. Speedy, R. J. & Angell, C. A. Isothermal compressibility of supercooled water and evidence for a thermodynamic singularity at −45°C. *J. Chem. Phys.* **65**, 851–858 (1976).
2. Tombari, E., Ferrari, C. & Salvetti, G. Heat capacity anomaly in a large sample of supercooled water. *Chem. Phys. Lett.* **300**, 749–751 (1999).
3. Matsumoto, M., Saito, S. & Ohmine, I. Molecular dynamics simulation of the ice nucleation and growth process leading to water freezing. *Nature* **416**, 409–413 (2002).
4. Molinero, V. & Moore, E. B. Water modeled as an intermediate element between carbon and silicon. *J. Phys. Chem. B* **113**, 4008–4016 (2009).
5. Koop, T., Luo, B. P., Tsias, A. & Peter, T. Water activity as the determinant for homogeneous ice nucleation in aqueous solutions. *Nature* **406**, 611–614 (2000).
6. Finney, J. L., Hallbrucker, A., Kohl, I., Soper, A. K. & Bowron, D. T. Structures of high and low density amorphous ice by neutron diffraction. *Phys. Rev. Lett.* **88**, 225503 (2002).
7. Moore, E. B. & Molinero, V. Growing correlation length in supercooled water. *J. Chem. Phys.* **130**, 244505 (2009).
8. Mallamace, F. *et al.* The anomalous behavior of the density of water in the range 30K < T 373K. *Proc. Natl Acad. Sci. USA* **104**, 18387–18391 (2007).
9. Johari, G. P., Fleissner, G., Hallburcker, A. & Mayer, E. Thermodynamic continuity between glassy and normal water. *J. Phys. Chem.* **98**, 4719–4725 (1994).
10. Huang, C. *et al.* Increasing correlation length in bulk supercooled HO, DO, and NaCl solution determined from small angle x-ray scattering. *J. Chem. Phys.* **133**, 134504 (2010).
11. Kohl, I., Mayer, E. & Hallbrucker, A. The glass water-cubic ice system: a comparative study by X-ray diffraction and differential scanning calorimetry. *Phys. Chem. Chem. Phys.* **2**, 1579–1586 (2000).
12. Stevenson, J. D. & Wolynes, P. G. The ultimate fate of supercooled liquids. *J. Phys. Chem. A* **115**, 3713–3719 (2011).
13. Moore, E. B., de la Llave, E., Welke, K., Scherlis, D. A. & Molinero, V. Freezing, melting and structure of ice in a hydrophilic nanopore. *Phys. Chem. Chem. Phys.* **12**, 4124–4134 (2010).
14. Jähnert, S. *et al.* Melting and freezing of water in cylindrical silica nanopores. *Phys. Chem. Chem. Phys.* **10**, 6039–6051 (2008).
15. Wedekind, J., Strey, R. & Reguera, D. New method to analyze simulations of activated processes. *J. Chem. Phys.* **126**, 134103 (2007).
16. Liu, J., Nicholson, C. E. & Cooper, S. J. Direct measurement of critical nucleus size in confined volumes. *Langmuir* **23**, 7286–7292 (2007).
17. Tanaka, H. Possible resolution of the Kauzmann paradox in supercooled liquids. *Phys. Rev. E* **68**, 011505 (2003).
18. Xu, L. *et al.* Appearance of a fractional Stokes-Einstein relation in water and a structural interpretation of its onset. *Nature Phys.* **5**, 565–569 (2009).
19. Kauzmann, W. The nature of the glassy state and the behavior of liquids at low temperatures. *Chem. Rev.* **43**, 219–256 (1948).
20. Kiselev, S. Physical limit of stability in supercooled liquids. *Int. J. Thermophys.* **22**, 1421–1433 (2001).
21. Angell, C. A. Insights into phases of liquid water from study of its unusual glass-forming properties. *Science* **319**, 582–587 (2008).
22. Speedy, R. J. Stability-limit conjecture — an interpretation of the properties of water. *J. Phys. Chem.* **86**, 982–991 (1982).
23. Poole, P. H., Sciortino, F., Essmann, U. & Stanley, H. E. Phase behaviour of metastable water. *Nature* **360**, 324–328 (1992).
24. Sastry, S., Debenedetti, P. G. & Sciortino, F. Singularity-free interpretation of the thermodynamics of supercooled water. *Phys. Rev. B* **53**, 6144–6154 (1996).
25. Mishima, O. & Stanley, H. E. The relationship between liquid, supercooled and glassy water. *Nature* **396**, 329–335 (1998).
26. Mishima, O. Application of polyamorphism in water to spontaneous crystallization of emulsified LiCl–H_2O solution. *J. Chem. Phys.* **123**, 154506 (2005).
27. Moore, E. B. & Molinero, V. Ice crystallization in water's "no-man's land". *J. Chem. Phys.* **132**, 244504 (2010).
28. Liu, Y., Panagiotopoulos, A. Z. & Debenedetti, P. G. Low-temperature fluid-phase behavior of ST2 water. *J. Chem. Phys.* **131**, 104508 (2009).
29. Limmer, D. T. & Chandler, D. The putative liquid-liquid transition is a liquid-solid transition in atomistic models of water. *J. Chem. Phys.* **135**, 134503 (2011).
30. Plimpton, S. J. Fast parallel algorithms for short-range molecular dynamics. *J. Comput. Phys.* **117**, 1–19 (1995).

Author Contributions V.M. conceived and designed the study and wrote the paper. E.B.M. and V.M. performed the simulations, analysed the data and interpreted the results.

Author Information Reprints and permissions information is available at www.nature.com/reprints. The authors declare no competing financial interests. Readers are welcome to comment on the online version of this article at www.nature.com/nature. Correspondence and requests for materials should be addressed to V.M. (Valeria.Molinero@utah.edu).

METHODS

Simulations. All molecular dynamics simulations were performed with LAMMPS[30]. Equations of motion were integrated using Velocity Verlet with a time step of 10 fs. Bulk simulations were conducted in the NpT ensemble, with $p = 1$ atm. Temperature and pressure were controlled with the Nose-Hoover thermostat and barostat, with time constants of 1 and 5 ps, respectively. The target temperature was decreased linearly in the cooling ramp simulations. Water was modelled with the mW potential[4]. Three different systems were used in this study: (1) the thermodynamics of bulk water was determined through cooling ramps with simulation cells containing 32,768 mW water molecules; (2) the isothermal crystallization simulations were performed with cells containing 4,096 mW water molecules, after checking that it produced consistent results with a simulation cell containing 13,768 molecules; and (3) the confined water system consisted of the 3 nm cylindrical nanopore used in the studies of ref. 31 and contained 2,123 water molecules embedded in a 5,840-molecule pore. The interactions between pore-wall and water are chosen to be as water with water, to minimize the effect of the pore-wall on the liquid[13]. The pore was headless to ensure that the crystallization occurs within the shaft of the pore. The pore was 90% filled to allow for expansion of the water as it is cooled and forms ice. The nanopore simulations were performed in the NVT ensemble, although it should be noted that the water inside is at zero pressure as the pore is not fully filled.

Thermodynamic properties. The enthalpy, $H = E + pV$, was directly computed along the simulation trajectories and saved every 0.2 ps or less and averaged over 100 ps running intervals. The heat capacity was obtained through numerical differentiation of H with respect to temperature. The excess entropy of liquid water with respect to ice (Supplementary Fig. 1) was obtained through integration of the change in entropy from the value at the melting point, $\Delta S_{m} = \Delta H_{m}/T_{m}$,

$$S^{ex}(T) = \Delta S_m(T_m) - \int_{T_m}^{T} \frac{c_p^{ex}(T')}{T'} dT'. \tag{1}$$

where the excess heat capacity of liquid with respect to ice is $c_p^{ex}(T') = c_p^{liquid}(T') - c_p^{ice}(T')$. $C_p^{ice}(T)$ was computed in ref. 32, as well as the excess free energy, $G^{ex} = H^{ex} - TS^{ex}$, that here we extend down to 150 K. We note that at temperatures lower than 205 K the liquid cannot be equilibrated and the thermodynamic properties depend on the rate of cooling, which determines the fraction of water that crystallizes to ice.

Identification of the ice nuclei. The CHILL algorithm[13] was used to distinguish between molecules with local order of liquid, ice I, and molecules with local ordering intermediate between that of ice and liquid, that here we call intermediate-ice and that we have called interfacial ice elsewhere[13,27], because it also forms on the interface between well defined crystallites and the liquid phase. An ice nucleus consists of clusters of molecules with any ice-like local environment, including both ice I and intermediate-ice. Ice nuclei are defined by clustering of ice and intermediate-ice molecules using 3.5 Å cut-off to define connected neighbours.

Crystallization simulations at constant temperature. To produce a large set (more than 100) of independent trajectories at each temperature, starting configurations were selected at 500 ps intervals from a single simulation at 300 K. From the starting configuration, the temperature was instantaneously quenched to the temperature of interest, T_{quench}, from 192 to 208 K, and the time was set to zero. The crystallization time, τ_{x}, is the time required to convert 70% of the water into ice. Nearly 1,000 simulations up to 350 ns in length each were collected. The crystallization time of mW water at 180 K was taken from ref. 27.

Nucleation times and critical nuclei size. We used the mean first passage time (MFPT) method as implemented in ref. 15 to determine the characteristic time-scale of nucleation. The number of water molecules in the largest ice nucleus, N, and its radius of gyration, R_{g}, were chosen as order parameters for the advance of the crystallization. The radius of gyration, R_{g}, and non-sphericity, NS, of the nuclei were determined as described in ref. 7. With the size of the ice nuclei as the order parameter, the nucleation time $\tau_{nucleation}$ and the critical nuclei size, N^{*}, can be determined. For a series of trajectories at a given temperature, the mean time of first appearance is recorded for the largest nucleus in each configuration. A plot of the MFPT, the time it takes for a given nucleus size, N, to grow rather than dissolve for the first time, versus nuclei size results in a sigmoidal curve that can be described by the following equation:[15]

$$\tau(N) = \frac{\tau_{nucleation}}{2} \left\{ 1 + erf[(N - N^{*})c] \right\} \tag{2}$$

where $\tau(N)$ is the MFPT as a function of cluster size, N, and c is a constant. The plateau of the sigmoidal curve gives the nucleation time, and the inflection point corresponds to the critical nucleus size, N^{*}.

Crystallization probability of individual nuclei. A series of simulations were run to compare the growth probabilities of selected nuclei of size predicted to be critical by the MFPT method based on radius of gyration. Configurations containing a potentially critically sized nucleus, with size N^{*}, were chosen and the R_{g} and NS of the nucleus were recorded. A series of 200 simulations were run from a set of independent configurations at 205 K, each initiated with newly randomized velocities, resulting in 200 unique simulations from each starting configuration. The probability of growth from the initial nucleus was calculated as the fraction of trajectories that resulted in nuclei growth after 5 ns, larger than the average growth time at 205 K, 2 ± 1 ns.

Local liquid environment of the nuclei. The liquid solvation shell of the crystalline clusters was analysed for the crystallization trajectories at 200 and 205 K. The shell was defined as the molecules of the liquid within 3.5 Å of any molecule of the crystal nucleus (the latter includes the intermediate-ice). We computed the ratio of four-coordinated (N_{4}) to higher-coordinated molecules (N_{H}) around the ice nuclei and compare it with the ratio for the whole system (which is about 40 times larger than the nuclei).

31. de La Llave, E., Molinero, V. & Scherlis, D. A. Water filling of hydrophilic nanopores. *J. Chem. Phys.* **133,** 034513 (2010).
32. Jacobson, L. C., Hujo, W. & Molinero, V. Thermodynamic stability and growth of guest-free clathrate hydrates: a low-density crystal phase of water. *J. Phys. Chem. B* **113,** 10298–10307 (2009).